Petroleum Science 19 (2022) 2649–2662

Contents lists available at ScienceDirect

Petroleum Science

journal homepage: www.keaipublishing.com/en/journals/petroleum-science

Original Paper

Theoretical dispersion curves for borehole real-valued wave modes in vertically transverse isotropic formations

Fu-Qiang Zeng [a, *], Chao Li [b, c]

[a] Hubei Subsurface Multi-scale Imaging Key Laboratory, Institute of Geophysics and Geomatics, China University of Geosciences, Wuhan, 430074, Hubei, China
[b] State Key Laboratory of Acoustics, Institute of Acoustics, Chinese Academy of Sciences, Beijing, 100190, China
[c] Beijing Engineering and Technology Research Center for Deep Drilling Exploration and Measurement, Beijing, 100190, China

ARTICLE INFO

Article history:
Received 6 November 2020
Accepted 28 October 2021
Available online 19 April 2022

Edited by Jie Hao

Keywords:
Dispersion equation
Scholte wave velocity
Acoustic properties
Transverse isotropy
Thomsen anisotropic parameters inversion

ABSTRACT

The dispersion curves of real-valued modes in a fluid-filled borehole are widely used in acoustic well logging. The accurate dispersion curves are the precondition of theoretical analysis and inversion process. Generally, these curves can be obtained by solving the conventional dispersion equation for isotropic formations and most vertically transverse isotropy (VTI) formations. However, if the real-valued solutions exist when the radial wavenumbers for the formation quasi-P and quasi-S equals to each other, the existed methods based on the conventional dispersion equation could lead to incorrect results for some VTI formations. Few studies have focused on the influence of these real-valued solutions on dispersion curve extraction. To remove these real-valued solutions, we have proposed a modified dispersion equation and its corresponding solving process. When solving the dispersion equation, the Scholte wave velocity of VTI formation at high frequency is used as the initial guess. The two synthetic examples including fast and slow VTI formations validate that these real-valued solutions do not contribute to the wavefield, and the new dispersion curve extraction method is suitable for all kinds of VTI formations. Consequently, the method can provide reliable dispersion curves for both theoretical analysis and anisotropic parameters inversion in VTI formations.

1. Introduction

Multipole acoustic well logging is widely used to reveal important mechanical properties of the formation around the borehole. Stoneley wave excited by a monopole source, flexural wave excited by a dipole source and screw wave excited by a quadrupole source are dispersive. These waveforms have been widely used in obtaining elastic parameters in geophysical exploration with the help of theoretical dispersion curves. For example, theoretical dispersion curves are critical to perform vertical compressional and vertical shear slowness inversion (e.g., Braunisch et al., 2004; Jiang et al., 2019), shear slowness profile inversion (e.g., Sunaga et al., 2009; Ma et al., 2013), and Thomsen anisotropy parameter inversion (e.g., Tang and Cheng, 2004; Xu et al., 2017, 2018; Zeng, 2019). These real-valued dispersion curves are non-radiating modes with no attenuation and contribute to whole wavefield, such as the Stoneley mode without leaky Stoneley mode included, flexural mode and screw mode without leaky screw mode included (Sinha and Asvadurov, 2004). The above methods are used under the assumption that the formation is transversely isotropic and can be described by five elastic constants (i.e., c_{11}, c_{13}, c_{33}, c_{44}, and c_{66}), also known as the Thomsen (1986) parameters (i.e. α, β, γ, δ, and ε). In this paper, the word "dispersion" is different from that used in porous rocks where the Biot theory formulations and Gassman equation are widely used (e.g., Tang and Cheng, 2004; Müller et al., 2010; Zhao et al., 2015, 2020, 2021).

These dispersion curves of real-valued wave modes from the conventional dispersion equation are solved by the Newton-Raphson method (Tang and Cheng, 2004) or the Levenberg-Marquardt method (Moré, 1978). Those methods are suitable for isotropic formations and most vertically transverse isotropy (VTI) formations with $\delta < \varepsilon$ or $\delta > \varepsilon + c_{44}/(2c_{33})$, where Thomsen

* Corresponding author.
E-mail addresses: JMichael@126.com (F.-Q. Zeng), chaolee_cupb@sina.com (C. Li).

https://doi.org/10.1016/j.petsci.2022.04.011

anisotropy parameters δ and ε are defined as $\frac{(c_{13}+c_{44})^2-(c_{33}-c_{44})^2}{2c_{33}(c_{33}-c_{44})}$ and $\frac{c_{11}-c_{33}}{2c_{33}}$ (Thomsen, 1986). However, when obtaining dispersion curves, real-valued solutions existed for certain VTI formations with $\varepsilon \le \delta < \varepsilon + c_{44}/(2c_{33})$ that do not represent any true wave mode, not contribute to the wavefield. He and Hu (2010) have proved that the wavefield is composed of the compressional wave and shear wave branch points, and poles for this kind of VTI formation. But they did not discuss on the influences of the real-valued solutions on solving the dispersion curve. These real-valued solutions might interfere with dispersion curve extraction and should be removed. These solutions are named as pseudo modes in this paper. Few studies have focused on the influence of these real-valued solutions on total wavefield, dispersion curve extraction and geophysical exploration. This paper can be regarded as an extension of their work.

In this paper, we propose a new method that can obtain real-valued dispersion curves of wave modes without the influence of pseudo modes. This method includes a modified dispersion equation and its corresponding solving process which is suitable for all VTI formations. We also use the synthetic examples to validate that pseudo modes do not contribute to the total wavefield but affect Thomsen anisotropy inversion. In addition, the method can be extended to both wireline and logging while drilling (LWD) acoustic logging when the instrument is taken into consideration.

2. Characteristics of theoretical dispersion curves

2.1. Pseudo modes of the dispersion equation

Multipole waves propagation in VTI formations in a fluid filled borehole have been analyzed in previous studies (e.g., Zhang et al., 1994; Tang and Cheng, 2004), and the coefficient of reflection A_f is based on the boundary conditions. The boundary conditions at the borehole interface are expressed as

$$\begin{cases} u = u_f \\ \sigma_{rr} = \sigma_{rrf} \\ \sigma_{rz} = 0 \\ \sigma_{r\theta} = 0 \end{cases}, \tag{1}$$

at $r = R$, where R is the borehole radius, u and u_f are radial displacement in formation and borehole fluid, σ_{rr} and σ_{rrf} are the radial stress in formation and borehole fluid, σ_{rz} and $\sigma_{r\theta}$ are shear stresses in the formation, respectively. The above boundary conditions lead to a matrix equation for the unknown coefficients:

$$\begin{pmatrix} M_{11} & M_{12} & M_{13} & M_{14} \\ M_{21} & M_{22} & M_{23} & M_{24} \\ 0 & M_{32} & M_{33} & M_{34} \\ 0 & M_{42} & M_{43} & M_{44} \end{pmatrix} \begin{pmatrix} A_f \\ B_n \\ D_n \\ F_n \end{pmatrix} = \begin{pmatrix} u_f^d \\ \sigma_{rrf}^d \\ 0 \\ 0 \end{pmatrix}, \tag{2}$$

where radial displacement u_f^d and stress u_{rrf}^d correspond to the direct wavefield in borehole fluid, B_n, D_n and F_n are coefficients associated with the modified Bessel function of the second kind at a given azimuth order number n, respectively, and M_{ij} are listed in Appendix A. The coefficient of reflection A_f in Eq. (2) is written as

$$A_f = \frac{N\left(k,\omega,n,R,\rho,\rho_f,\alpha_f,c_{11},c_{13},c_{33},c_{44},c_{66}\right)}{D\left(k,\omega,n,R,\rho,\rho_f,\alpha_f,c_{11},c_{13},c_{33},c_{44},c_{66}\right)}, \tag{3}$$

where N and D are the determinates of matrixes defined in Appendix A, whose elements M_{i2} and M_{i4} are different from conventional elements (Tang and Cheng, 2004) and other elements are the same as conventional elements; k is the wavenumber in the direction of wave propagation; ω is the angular frequency; the azimuthal order number n controls the azimuthal variation of the wavefield with $n = 0$, 1 and 2 corresponding to monopole, dipole and quadrupole modes, respectively; ρ is the formation density; ρ_f and α_f are the borehole fluid density and velocity, respectively. The vertical compressional velocity α and vertical shear velocity β are defined as $\alpha = \sqrt{c_{33}/\rho}$, and $\beta = \sqrt{c_{44}/\rho}$, respectively. The elements M_{i2} and M_{i4} are different from ones in the conventional dispersion equation (Tang and Cheng, 2004). $(q_P^2 - k^2)/(c_{44}k^2 - (c_{11} - c_{13} - c_{44})q_P^2 - \rho\omega^2)$ and $(k^2 - q_{SV}^2)/((c_{13} + 2c_{44})k^2 - c_{11}q_{SV}^2 - \rho\omega^2)$ are the common factors of M_{i2} and M_{i4} in the conventional dispersion equation, respectively. For the traditional dispersion equation, solutions satisfying $q_P^2 - k^2 = 0$ and $q_{SV}^2 - k^2 = 0$ do not represent any wave motion (Tang and Cheng, 2004). The influence of real-valued solutions related to it can be avoided by solving Eq. (4),

$$D\left(k,\omega,n,R,\rho,\rho_f,\alpha_f,c_{11},c_{13},c_{33},c_{44},c_{66}\right) = 0, \tag{4}$$

Similarly, if $q_P = q_{SV}$, M_{i4} will be equal to ikM_{i2}, and the solutions related to it will make the denominator of A_f zero in some VTI formation. Existed studies (He and Hu, 2009, 2010) have proved that the solutions related to $q_P = q_{SV}$, are branch points not poles for those VTI formations with $\delta > \varepsilon + c_{33}/(2c_{44})$. Similar to the influence of the borehole fluid velocity on dispersion curve extraction of flexural wave, if the solutions related to $q_P = q_{SV}$, are real-valued, it might interfere the dispersion curve extraction. When solving Eq. (4), the real-valued solutions related to $q_P = q_{SV}$ should be identified whether they affect dispersion extraction. It is obvious that it requires

$$V^2 - 4UW = 0, \tag{5}$$

which can be simplified as

$$a(\omega/k)^4 + b(\omega/k)^2 + c = 0, \tag{6}$$

where

$$\begin{aligned} a &= \rho^2(c_{11} - c_{44})^2,\ b \\ &= 2\rho\left({c_{13}}^2 + 2c_{13}c_{44} - c_{11}c_{33}\right)(c_{44} + c_{11}) + 4\rho(c_{44} \\ &\quad + c_{33})c_{11}c_{44},\ \text{and}\ c \\ &= \left(c_{13}^2 + 2c_{13}c_{44} - c_{11}c_{33}\right)^2 - 4c_{11}c_{33}c_{44}^2. \end{aligned}$$

The two solutions from Eq. (6) are

$$\alpha_1 = \omega \Big/ k_1 = \sqrt{\left(-b + \sqrt{b^2 - 4ac}\right)\Big/(2a)},$$

$$\alpha_2 = \omega \Big/ k_2 = \sqrt{\left(-b - \sqrt{b^2 - 4ac}\right)\Big/(2a)}. \tag{7}$$

If $b^2 - 4ac \ge 0$ and $-b + \sqrt{b^2 - 4ac} > 0$, α_1 will be real-valued; if $b^2 - 4ac \ge 0$ and $-b - \sqrt{b^2 - 4ac} > 0$, α_2 will also be real-valued. α_1 and α_2 are smaller than β if they are real-valued.

Existing studies (He and Hu, 2009, 2010) have proven that $\pm k_1$

and $\pm k_2$ are branch points of a VTI formation with $\delta > \varepsilon + c_{44}/(2c_{33})$; the imaginary-valued $\pm k_2$ does not affect real-valued dispersion extraction; α_1 is the asymptotic velocity of flexural mode. The influence of solution α_1 on dispersion extraction can be effectively removed when computing the dispersion curves from high frequency for this type of VTI formation. However, for VTI formations with $\varepsilon \le \delta < \varepsilon + c_{44}/(2c_{33})$ where $\varepsilon \le \delta$ is deduced from $b^2 - 4ac \ge 0$, k_1 or k_2 does not make any contribution to the total wavefield. It should be noted that k_1 or k_2 are not always complex, which is different from He and Hu (2010). The rea-valued solutions of $q_P = q_{SV}$ might affect dispersion extraction and the removal of real-valued solutions of $q_P = q_{SV}$ helps to perform dispersion curve extraction. The real-valued α_1 and α_2 are named as pseudo modes in this paper.

2.2. The low-frequency asymptotes of all real-valued wave modes

The low-frequency asymptote of a real-valued wave mode can be used to check whether the cut-off frequency exists. It's true that the low-frequency asymptote of Stoneley wave mode exists. But for the first order flexural wave mode, the findings of existing studies are not consistent (e.g., Schmitt, 1988; Tang and Cheng, 2004; Zhang et al., 2009; Xu et al., 2017).

Considering the asymptotic expansion for the modified Bessel functions of the first and second kind (Zhang and Jin, 2011), when $\omega \to 0$, M_{ij} can be simplified as M_{ij}^0 expressed in Appendix B. The determinant of $|M_{ij}|$ can be

$$E_0(v) = |M_{ij}|, \tag{8}$$

where, $v = \omega/k$, is the phase velocity. Eq. (8) can be used to determine the low-frequency asymptotes of all real-valued wave modes. For $E_0(v) = 0$, there will be less than or equal to three real-valued solutions in $(0,\ \beta)$, including v_0, α_1 and α_2. For azimuth order number $n = 0$, v_0 is equal to the low-frequency asymptote of Stoneley wave mode (White and Sengbush, 1953); for $n = 1$, v_0 is equal to the low-frequency asymptote of the first order flexural mode; for $n > 1$, there is less than two real-valued solutions in $(0,\ \beta)$, including α_1 and α_2. The low-frequency asymptote v_0 can be determined by minimizing the following cost function:

$$E_1(v) = \begin{cases} E_0(v) \Big/ \left(v_{\alpha_1}^r v_{\alpha_2}^r\right) & \alpha_1, \alpha_2 > 0 \\ E_0(v) \Big/ \left(v_{\alpha_1}^r\right) & \alpha_1 > 0, \alpha_2 = 0 \quad \text{or} \quad \alpha_2 \in \mathbb{C} \\ E_0(v) \Big/ \left(v_{\alpha_2}^r\right) & \alpha_2 > 0, \alpha_1 = 0 \quad \text{or} \quad \alpha_1 \in \mathbb{C} \\ E_0(v) & \alpha_{1(2)} = 0 \quad \text{or} \quad \alpha_{1(2)} \in \mathbb{C} \end{cases} \tag{9}$$

where $v_{\alpha_1}^r = \sqrt{1/v^2 - 1/\alpha_1^2}$, $v_{\alpha_2}^r = \sqrt{1/v^2 - 1/\alpha_2^2}$.

2.3. The high-frequency asymptote of all real-valued wave modes

The high-frequency asymptote of all real-valued wave modes coincides with Scholte-wave velocity v_{Sch} (the speed of a surface wave along a planar fluid-solid interface at high frequency). Many studies (e.g., Braunisch et al., 2004; Vinh, 2013; Fang and Cheng, 2018) have focused on the isotropic formation. The Scholte-wave velocity can be used in borehole fluid velocity inversion (Valero et al., 2009) and formation shear velocity inversion (Zhang et al., 2019).

Considering the asymptotic expansion for the modified Bessel functions of the first and second kind (Zhang and Jin, 2011), $K_n(z) \sim \sqrt{\frac{\pi}{2z}} e^{-z}$, and $I_n(z) \sim \frac{e^z}{\sqrt{2\pi z}}$, which is valid for large $|z|$. When $\omega \to \infty$, M_{ij} after removing common factors can be simplified as M_{ij}^∞, whose elements with non-zero values are

$$\begin{aligned}
M_{11}^\infty &= -v_f^r \\
M_{12}^\infty &= -i(c_{13} + c_{44}) v_P^r / v \\
M_{14}^\infty &= -i(c_{13} + c_{44}) v_{SV}^r / v \\
M_{21}^\infty &= \rho_f \\
M_{22}^\infty &= i\left[c_{11}c_{44}(v_P^r)^2 + c_{13}\left(c_{44} \Big/ v^2 - \rho\right)\right] \Big/ v \\
M_{24}^\infty &= i\left[c_{11}c_{44}(v_{SV}^r)^2 + c_{13}\left(c_{44} \Big/ v^2 - \rho\right)\right] \Big/ v \\
M_{33}^\infty &= \rho - c_{44} \Big/ v^2 \\
M_{42}^\infty &= c_{44}\left[c_{13} \Big/ v^2 + c_{11}(v_P^r)^2 + \rho\right] v_P^r \\
M_{44}^\infty &= c_{44}\left[c_{13} \Big/ v^2 + c_{11}(v_{SV}^r)^2 + \rho\right] v_{SV}^r
\end{aligned} \tag{10}$$

where, v is the phase velocity,

$$v_f^r = \sqrt{1/v^2 - 1/\alpha_f^2},\ v_P^r = \sqrt{\left(-V_\infty + \sqrt{V_\infty^2 - 4UW_\infty}\right) \Big/ (2U)},$$
$$v_{SV}^r = \sqrt{\left(-V_\infty - \sqrt{V_\infty^2 - 4UW_\infty}\right) \Big/ (2U)}$$

$$V_\infty = \rho(c_{11} + c_{44}) + \left(c_{13}^2 + 2c_{13}c_{44} - c_{11}c_{33}\right) \Big/ v^2,\ W_\infty = \left(\rho - c_{44} \Big/ v^2\right)\left(\rho - c_{33} \Big/ v^2\right).$$

So, the determinant of $|M_{ij}|$ can be

$$|M_{ij}| = M_{33}^\infty \begin{vmatrix} M_{11}^\infty & M_{12}^\infty & M_{14}^\infty \\ M_{21}^\infty & M_{22}^\infty & M_{24}^\infty \\ 0 & M_{42}^\infty & M_{44}^\infty \end{vmatrix} = M_{33}^\infty F_0(v) \tag{11}$$

with $F_0(v) = M_{11}^\infty (M_{22}^\infty M_{44}^\infty - M_{24}^\infty M_{42}^\infty) + M_{21}^\infty (M_{42}^\infty M_{14}^\infty - M_{12}^\infty M_{44}^\infty)$.

Eq. (11) is independent of , R, ω and c_{66}. For $F_0(v) = 0$, there are less than or equal to four real-valued solutions in $(0,\ \beta)$, including v_{Sch}, β, α_1 and α_2. The Scholte-wave velocity is dependent on c_{11}, c_{33}, c_{13}, c_{44}, ρ, ρ_f and α_f, but not dependent on c_{66}, which has not been reported in previous studies (e.g., Braunisch et al., 2004).

However, there is no common extract root formula for five and above power equations (Shmakov, 2011). Therefore, the Scholte-wave velocity will be determined by minimizing the following cost function:

$$F_1(v)=\begin{cases} F_0(v)\Big/\left(v_S^r v_{\alpha_1}^r v_{\alpha_2}^r\right) & \alpha_1,\alpha_2>0 \\ F_0(v)\Big/\left(v_S^r v_{\alpha_1}^r\right) & \alpha_1>0,\alpha_2=0 \quad \text{or} \quad \alpha_2\in C \\ F_0(v)\Big/\left(v_S^r v_{\alpha_2}^r\right) & \alpha_2>0,\alpha_1=0 \quad \text{or} \quad \alpha_1\in C \\ F_0(v)/v_S^r & \alpha_{1(2)}=0 \quad \text{or} \quad \alpha_{1(2)}\in C \end{cases} \tag{12}$$

where $v_S^r=\sqrt{c_{44}/v^2-\rho}$. Eq. (12) can remove the influence of β, α_1 and α_2. The Scholte-wave velocity can be found in $(0,\ \beta)$ for slow formation or $\left(0,\ \alpha_f\right)$ for fast formation by the brute force grid search (Press et al., 2007) or a global minimization algorithm, such as the very fast simulated annealing algorithm (Ingber, 1989). The Scholte-wave velocity can be used as the initial guess when computing dispersion curves starting from high frequencies in a short velocity band with Scholte-wave velocity included by the Newton-Raphson method (Tang and Cheng, 2004) or the Levenberg-Marquardt method (Moré, 1978). The solution at the given frequency would be close to the Scholte-wave velocity. Generally, the velocity for the Stoneley wave mode at high frequency is smaller than Scholte-wave velocity; the velocities for the flexural wave mode and screw wave mode at high frequency is larger than Scholte-wave velocity.

2.4. Theoretical dispersion extraction of real-valued wave modes

For the real-valued wave modes, the dispersion curve can be computed by the Newton-Raphson method (Tang and Cheng, 2004) or the Levenberg-Marquardt method (Moré, 1978) from the following equation:

$$D_1(v,\omega)=0, \tag{13}$$

with

Table 1
Parameters for a water-filled borehole in two VTI formations. The real-valued solutions of pseudo modes and Scholte wave velocity are also included.

	ρ, kg/m^3	α, m/s	β, m/s	ε	γ	δ	v_{Sch}, m/s	α_1, m/s
Bandera sandstone	2160	3810	2368	0.03	0.03	0.045	1465.71	1815.91
Pierre shale 950	2250	2202	969	0.015	0.03	0.06	828.55	927.21

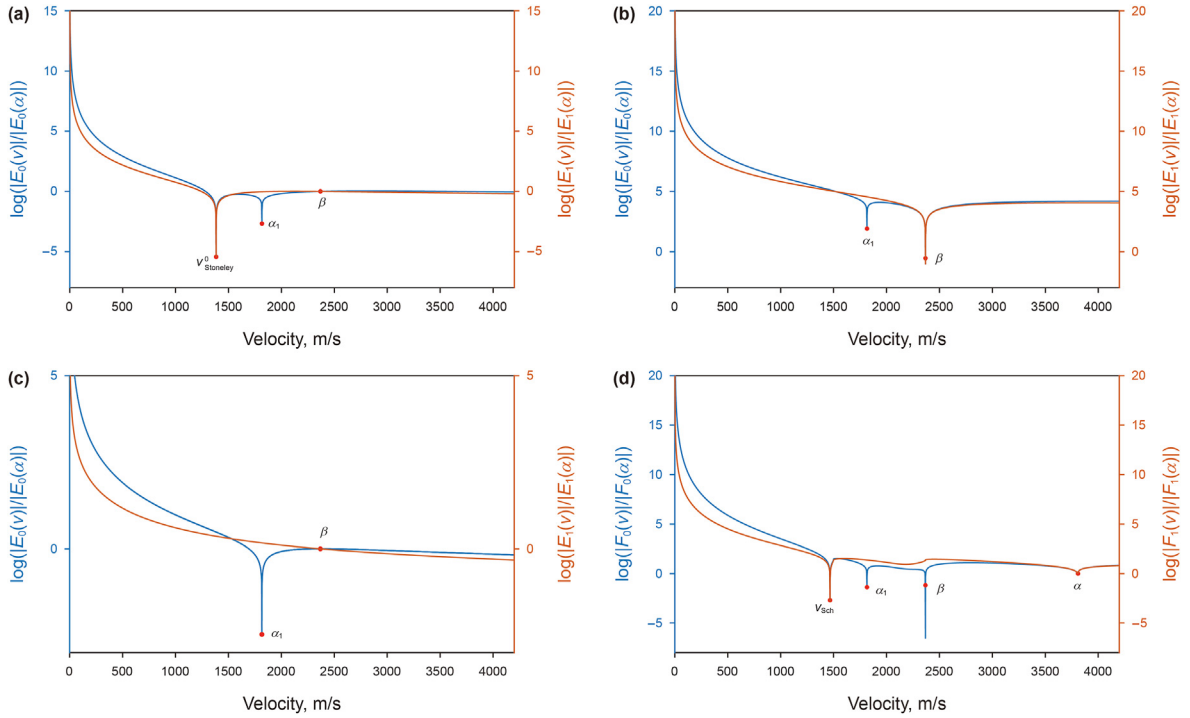

Fig. 1. Bandera sandstone. Solutions of $E_0(v)=0$ and $E_1(v)=0$ at 0.01 Hz for monopole (a), for dipole (b) and for quadrupole (c); (d) solutions of $F_0(v)=0$ and $F_1(v)=0$ when $\omega\to\infty$.

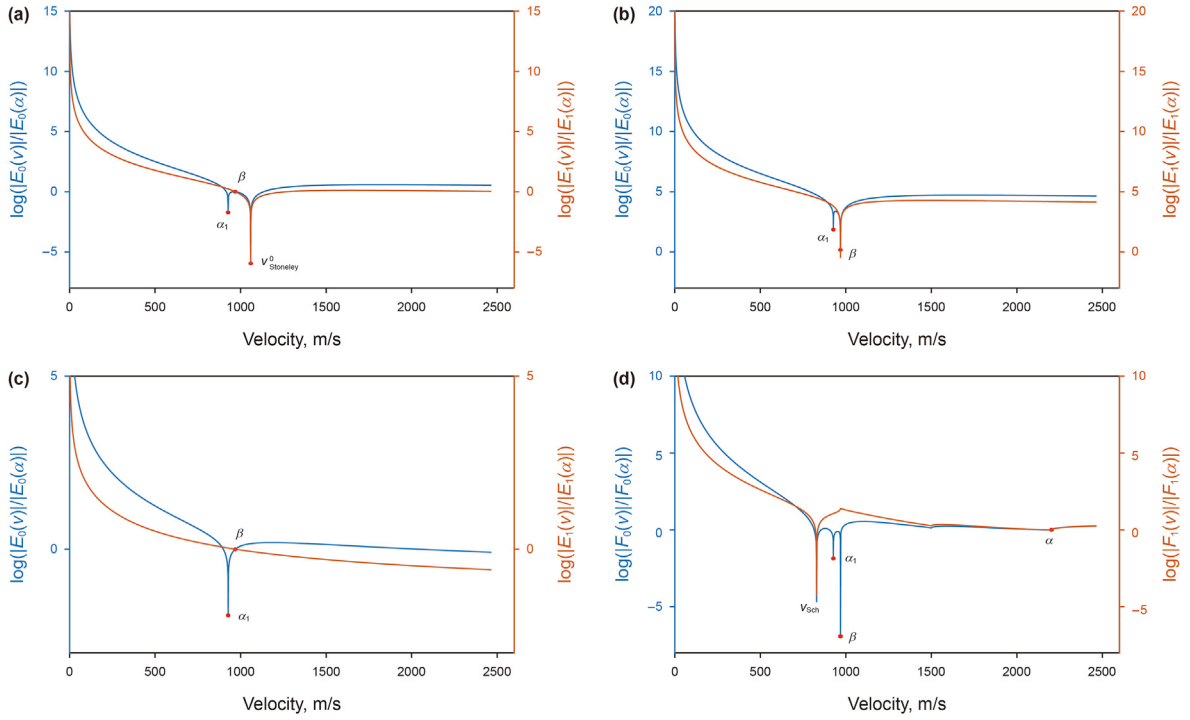

Fig. 2. Pierre shale 950. Solutions of $E_0(v)=0$ and $E_1(v)=0$ at 0.01 Hz for monopole (a), for dipole (b) and for quadrupole (c); (d) solutions of $F_0(v)=0$ and $F_1(v)=0$ when $\omega\to\infty$.

$$D_1(v,\omega)=\begin{cases} D_0(v,\omega)\Big/\left(\left(v_f^r\right)^n v_{\alpha_1}^r v_{\alpha_2}^r\right) & \alpha_1,\alpha_2>0 \\ D_0(v,\omega)\Big/\left(\left(v_f^r\right)^n v_{\alpha_1}^r\right) & \alpha_1>0,\alpha_2=0 \quad \text{or} \quad \alpha_2\in\mathbb{C} \\ D_0(v,\omega)\Big/\left(\left(v_f^r\right)^n v_{\alpha_2}^r\right) & \alpha_2>0,\alpha_1=0 \quad \text{or} \quad \alpha_1\in\mathbb{C} \\ D_0(v,\omega)\Big/\left(v_f^r\right)^n & \alpha_{1(2)}=0 \quad \text{or} \quad \alpha_{1(2)}\in\mathbb{C} \end{cases}, \text{if } \delta\le\varepsilon+c_{44}\Big/(2c_{33});$$

$$D_1(v,\omega)=D_0(v,\omega)\Big/\left(v_f^r\right)^n, \text{ if } \delta>\varepsilon+c_{44}\Big/(2c_{33})$$

and $D_0(v,\omega)=D(k,\omega,n,R,\rho,\rho_f,\alpha_f,c_{11},c_{13},c_{33},c_{44},c_{66})$.

Considering the asymptotic expansion for the modified Bessel functions of the first kind $I_n(z)$ with small z in M_{i1} (Zhang and Jin, 2011), the influence of borehole fluid velocity can be removed for $n>0$. Eq. (13) can remove all real-valued pseudo modes of all VTI formations.

The detailed numerical algorithm consists of the following steps. The first step is to obtain Scholte-wave velocity by Eq. (12) with the help of the brute force grid search (Press et al., 2007) or a global minimization algorithm, such as the very fast simulated annealing algorithm (Ingber, 1989). The second step is to obtain the velocity of a given mode at high frequency with the Scholte-wave velocity used as the initial guess in a short velocity band with Scholte-wave velocity included by the Newton-Raphson method (Tang and Cheng, 2004) or the Levenberg-Marquardt method (Moré, 1978). The third step is to use the previous solution at high frequency as an initial guess at the next frequency. The fourth step is to repeat the third step for all frequencies until all roots are found from high frequency to low frequency.

3. Examples

In this section, Bandera sandstone and Pierre shale 950 (Thomsen, 1986) in Table 1 are used to demonstrate the influence of pseudo modes on dispersion curves of real-valued wave modes, waveforms, and Thomsen anisotropy parameters inversion of a VTI formation. The Bandera sandstone is a fast formation whose vertical shear velocity is larger than compressional velocity of borehole fluid; and Pierre shale 950 is a slow formation whose vertical shear velocity is smaller than compressional velocity of borehole fluid. The density ρ_f and compressional velocity α_f of borehole fluid are 1000 kg/m^3 and 1500 m/s, respectively. The borehole radius is

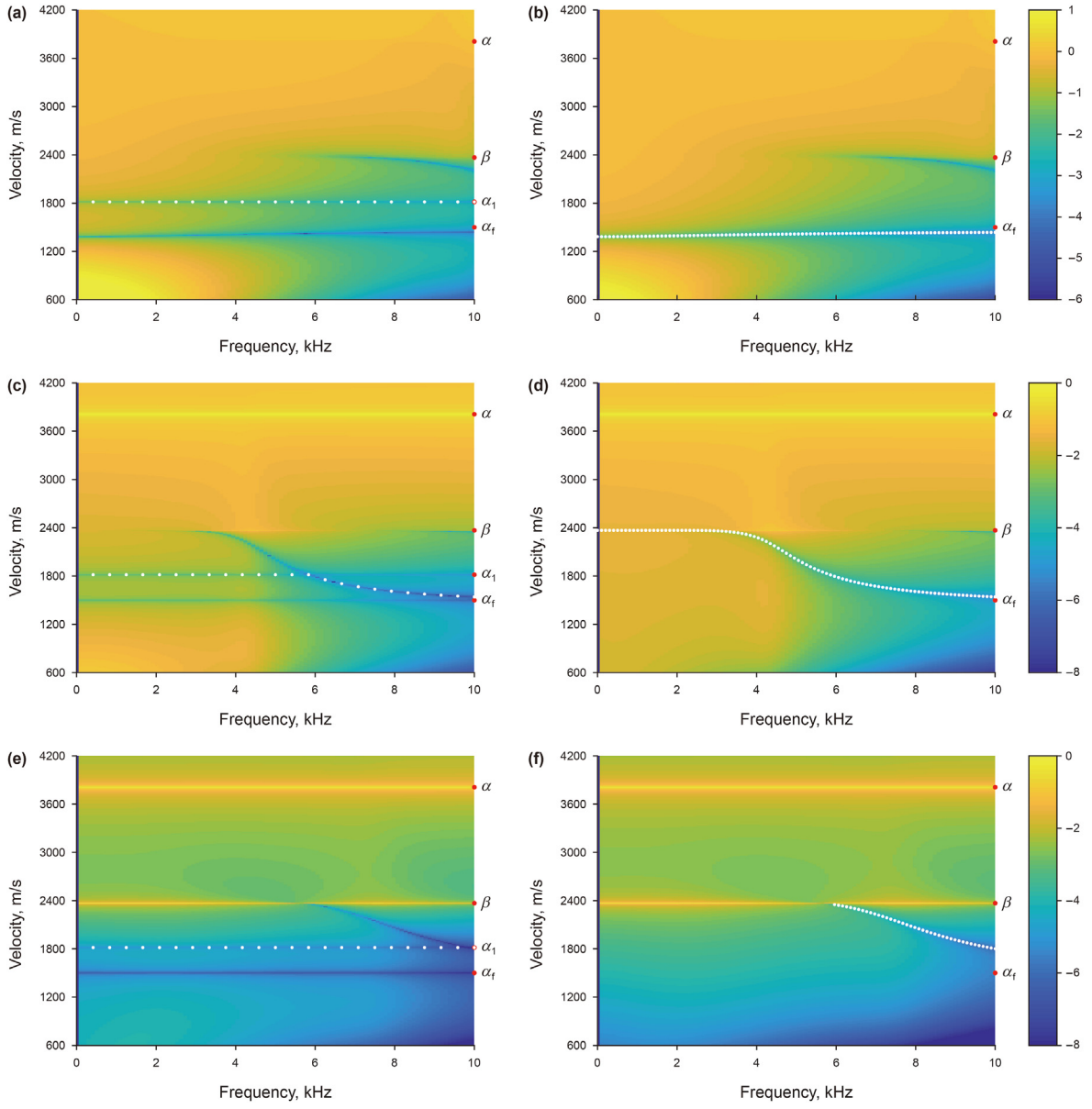

Fig. 3. Bandera sandstone. Objective residuals of $D_0(v,\ \omega)$ for monopole mode (a), dipole mode (c), quadrupole mode (e) and $D_1(v,\ \omega)$ for monopole mode (b), dipole mode (d), quadrupole mode (f).

0.1016 m. The Scholte-wave velocity in Table 1 from Eq. (12) is less than α_f. The synthetic waveforms of monopole, dipole and quadrupole are computed by real axis integration (RAI) method (Tsang and Radar, 1979). The source $S(t)$ with a pulse width T_w (0.5 ms) and a variable center frequency f_0 is used as follows:

$$S(t)=\begin{cases}\dfrac{1}{2}\left[1+\cos\dfrac{2\pi}{T_w}\left(t-\dfrac{T_w}{2}\right)\right]\cos 2\pi f_0\left(t-\dfrac{T_w}{2}\right), & 0\le t\le T_w\\ 0, & t>T_w\end{cases} \tag{14}$$

For the fast formation, f_0 for monopole, dipole and quadrupole sources are 6.0 kHz, 3.0 kHz and 6.0 kHz, respectively; for the slow formation, f_0 for monopole, dipole and quadrupole sources are 6.0 kHz. The source-to-receiver axial distances are from 2.0 to 4.0 m with an equal interval of 0.1 m.

3.1. Theoretical dispersion curves

In acoustic logging, the dispersion curves of real-valued wave modes are widely used in geophysical exploration. Figs. 1–2 show the low-frequency and high-frequency asymptotes of real-valued wave modes for Bandera sandstone and Pierre shale 950, respectively. The Stoneley wave velocity at 0.01 Hz of $E_1(v)=0$ and $E_0(v)=0$ coincides with its low-frequency asymptote $v^0_{Stoneley}$. The

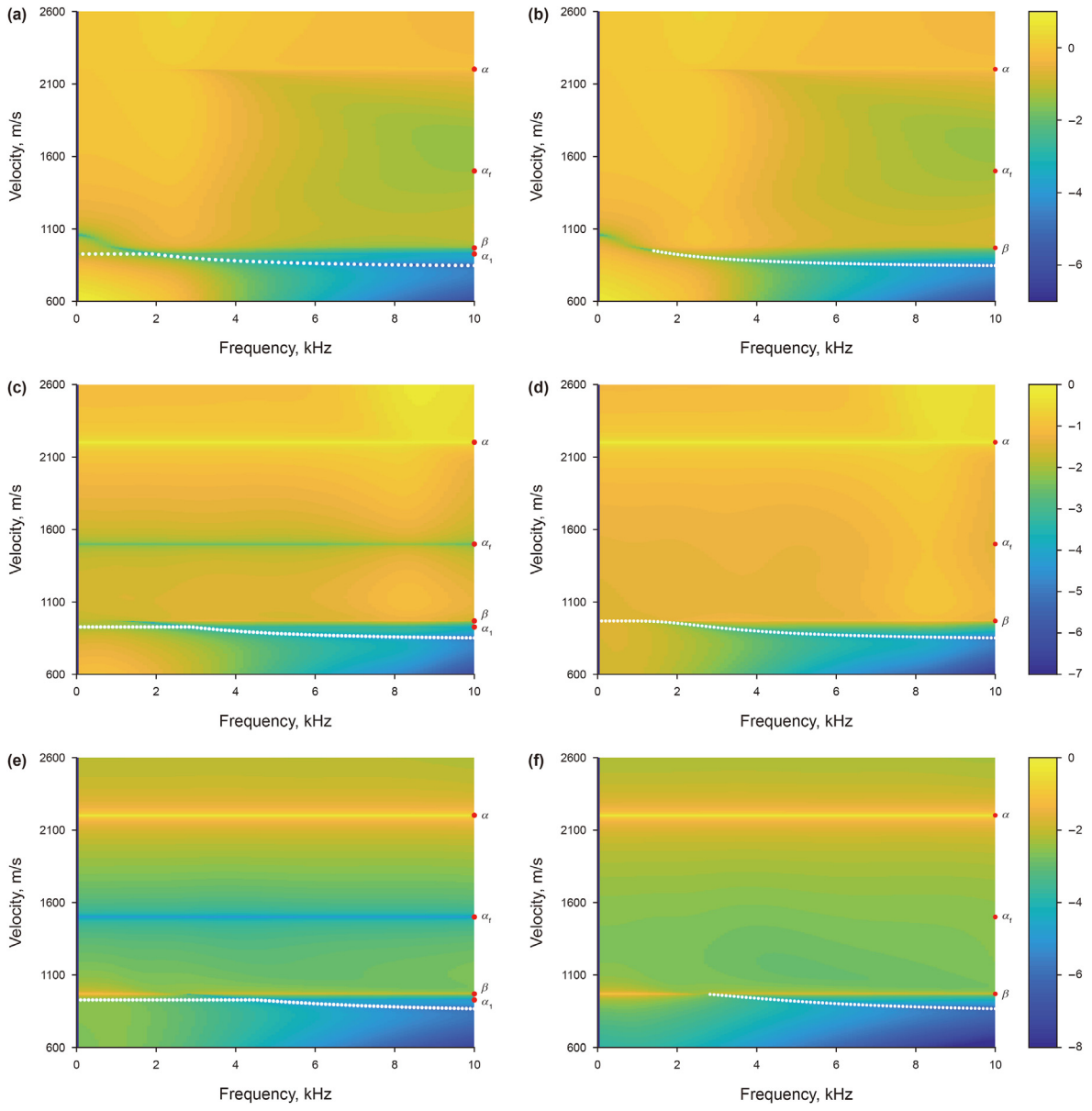

Fig. 4. Pierre shale 950. Objective residuals of $D_0(v,\ \omega)$ for monopole mode (a), dipole mode (c), quadrupole mode (e) and $D_1(v,\ \omega)$ for monopole mode (b), dipole mode (d), quadrupole mode (f).

solutions of shear velocity β in $E_1(v) = 0$ and $E_0(v) = 0$ indicate that the cut-off frequency of the flexural wave mode does not exist, which coincides with existing studies. Figs. 1(c) and 2(c) show that the cut-off frequency of the screw wave mode exists. Figs. 1(d) and 2(d) show the Scholte-wave velocity v_{Sch} can be obtained by solving $F_0(v) = 0$ and $F_1(v) = 0$, and v_{Sch} is the only solution of $F_1(v) = 0$ in $(0,\ \beta)$. Figs. 1–2 show that pseudo mode α_1 exists in the whole frequency domain, but the influence of α_1 can be successfully removed if Eqs. (9) and (12) is used.

The roots of $D_1(v) = 0$ and $D_0(v) = 0$ are located in the minima of the error surface. For the Bandera sandstone and Pierre shale 950, α_1 and α_2 are real-valued and complex, respectively. Figs. 3–4 both show that dispersion curves of real-valued wave modes (white dot lines) are wrong if Eq. (4) is used but they can be correctly obtained by solving Eq. (13) which can remove the influence of pseudo mode and borehole fluid wave mode. For example, the wrong dispersion curve of flexural wave in Fig. 3(c) is explained as follows. Firstly, interference of α_1 exists in whole frequency domain; secondly, the dispersion curve is obtained by using the previous solution at a higher frequency as the initial guess; and finally, it's hard to identify which solution is correct for the flexural wave mode. The dispersion curve can be obtained by solving Eq. (13) in Fig. 3(d) if the first solution at 10.0 kHz is correct for the flexural wave mode without the interference of pseudo modes.

3.2. Synthetic waveforms

As described previous section, the pseudo modes do not

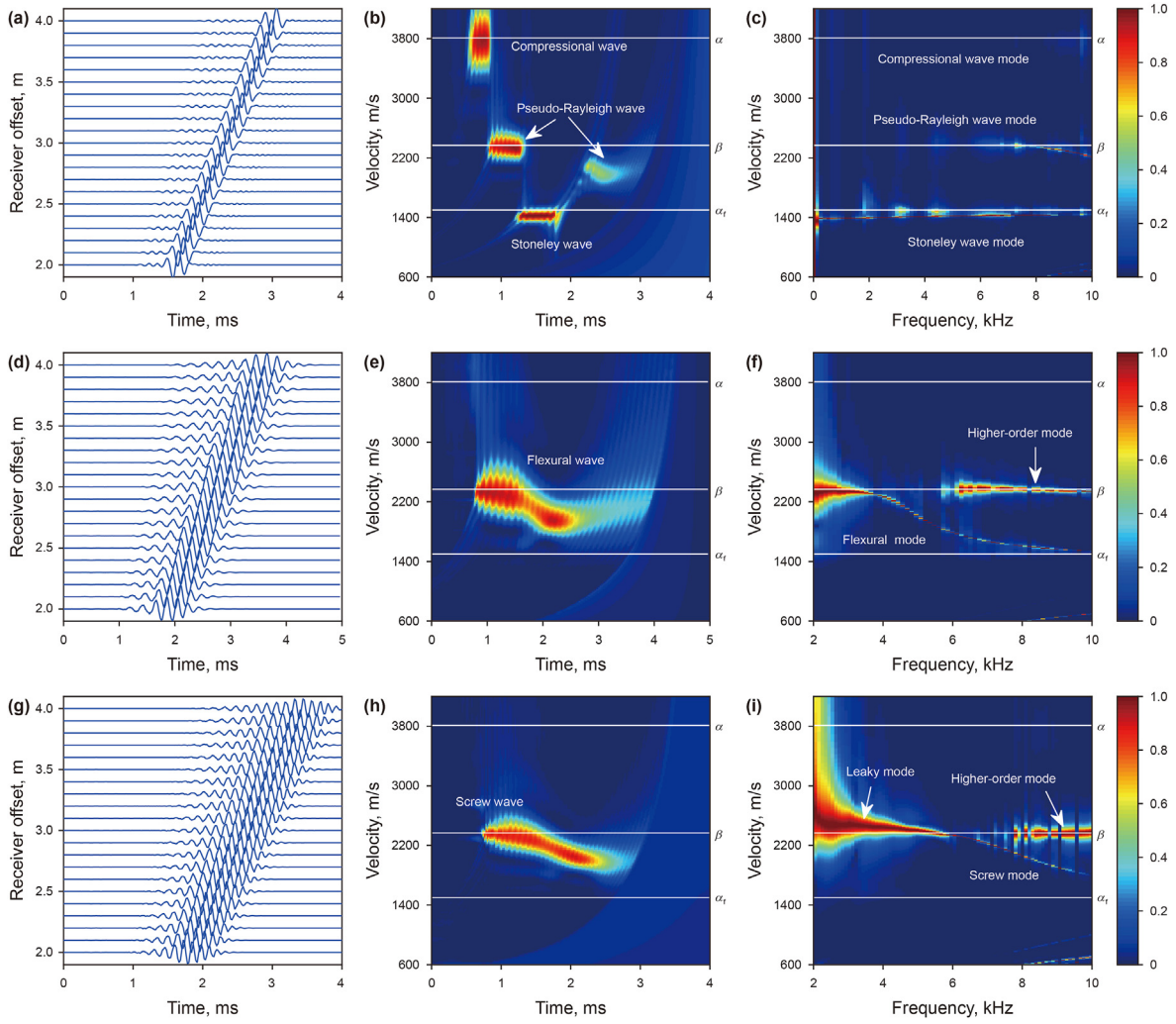

Fig. 5. Bandera sandstone. (a) Synthetic waveforms, (b) STC result and (c) FBAPES result for monopole case; (d)–(f) for dipole case; (g)–(i) for quadrupole case.

contribute to the total wavefield. It can also be validated by processing the synthetic waveforms in time and frequency domain, i.e., the slowness-time coherence (STC) (Kimball, 1986) result and dispersion analysis by the forward and backward amplitude and phase estimation (FBAPES) (Li et al., 2015) method which can identify all wave modes. For Bandera sandstone, Fig. 5(a) and (d) and 5(g) show the synthetic monopole, dipole and quadrupole waveforms, respectively. The compressional wave mode, pseudo-Rayleigh wave mode and Stoneley wave mode in Fig. 5(b) and (c) can be found. Fig. 5(e) show that the flexural wave is dispersive, which is validated by the dispersion analysis result of the flexural wave mode and its higher-order mode in Fig. 5(f). Unlike the monopole case, there is a leaky mode in Fig. 5(i) except the real-valued screw mode and its higher-order mode. It's obvious that the pseudo mode does not appear in Fig. 5(b)-5(c), 5(e)-5(f) and 5(h)-5(i), which also proves that k_1 is a removable branch point and does not contribute to the total wavefield. For Pierre shale 950, Fig. 6 shows the synthetic monopole, dipole and quadrupole waveforms and results processed by STC and dispersion analysis, which also proves that k_1 does not contribute to the total wavefield. Different from Bandera sandstone, results by STC and dispersion analysis show that the borehole fluid signal appears in synthetic waveforms; the borehole fluid signal should not appear. The appearance of the borehole fluid signal is from the RAI method using sum of direct wavefield and reflected wavefield which does not remove the influence of borehole fluid exactly.

3.3. Influence on thomsen anisotropic parameters inversion

Thomsen anisotropic parameters are very important and can be obtained by processing dispersion data. The Thomsen anisotropy parameters is obtained by

$$Obj(\delta,\gamma)=\log_{10}\int_{\Omega}|v_m(\omega;\delta,\gamma)-v_d(\omega)|^2\mathrm{d}\omega, \tag{15}$$

where v_m and v_d denote the calculated velocity dispersion curve and the processed dipole dispersion data, respectively. For Bandera sandstone, $\gamma=\varepsilon$ is used in Eq. (15); for Pierre shale 950, ε is assumed to be known. Both are used to investigate the influence of pseudo modes on Thomsen anisotropic parameters inversion. The processing frequency band Ω is selected as $[(f_{Airy}-1)\ \text{kHz},\ (f_{Airy}+1)\ \text{kHz}]$ where f_{Airy} is the Airy frequency. For Bandera sandstone, f_{Airy} is 4.6 kHz; for Pierre shale 950, f_{Airy} is 2.4 kHz. Obviously, Eq. (15) is dependent on the accuracy of v_m. As described previous section, it's possible to encounter the interference of the pseudo modes when Eq. (4) is used. For the VTI formations in Table 1, area (1) holding $\delta>\varepsilon+c_{44}/(2c_{33})$ in Figs. 7(a)

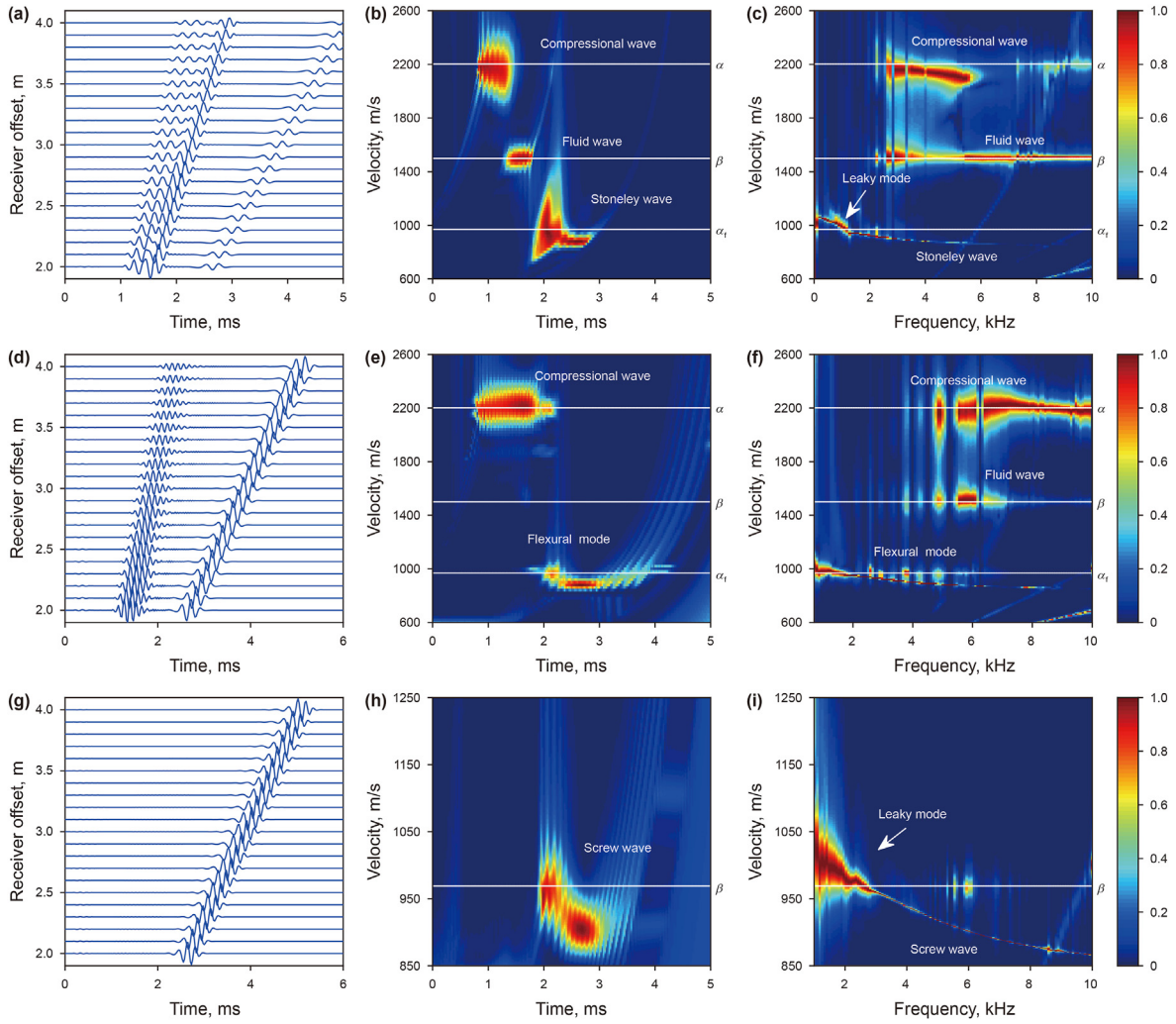

Fig. 6. Pierre shale 950. (a) Synthetic waveforms, (b) STC result and (c) FBAPES result for monopole case; (d)–(f) for dipole case; (g)–(i) for quadrupole case.

and 8(a) show that it's impossible to find the true solution in this area but in areas (2) and (3) holding $\delta < \varepsilon + c_{44}/(2c_{33})$ can be used as searching area of Eq. (15). There will be pseudo modes interference due to real-valued solutions related to $q_P = q_{SV}$ in area (2), and no pseudo modes interference in area (3). The red points in Fig. 7(a)-7(c), 7(e), 8(a)-8(c) and 8(e) are the true solution of $Obj(\delta, \gamma) = 0$. Fig. 7(c), (e), 8(c) and 8(e) show that it's necessary to calculate the dispersion curves by Eq. (13) not Eq. (4). Obviously, the solution of $Obj(\delta, \gamma) = 0$ with dispersion curves determined by Eq. (4) will be found in area (1) not area (2) of Figs. 7(e) and 8(e). The main reason is that some dispersion curves with frequency less than the red line in Figs. 7(f) and 8(f) are not correctly obtained.

4. Discussion

The rock samples collected by Thomsen (1986) can be divided into two parts by the relation between δ and $\varepsilon + c_{44}/(2c_{33})$. For VTI formations with $\delta > \varepsilon + c_{44}/(2c_{33})$, the solution α_2 is an imaginary value. The dispersion curves can be obtained correctly by solving Eq. (13) from high frequency. The influence of α_1 can be avoided. For those VTI formations with $\delta \leq \varepsilon + c_{44}/(2c_{33})$, there are 14 rock samples with α_1 real-valued and α_2 complex. The dispersion curves of real-valued wave modes for the remaining rock samples can be obtained by traditional methods because α_1 and α_2 are complex. α_1 and α_2 are also complex for other published rock samples (e.g., Table 1 of Wang, 2002; Tang and Cheng, 2004; Sunaga et al., 2009; Li et al., 2013).

The Thomsen anisotropy parameters of 237 rock samples with c_{66} measured by Wang (2002) all satisfy $\delta \leq \varepsilon + c_{44}/(2c_{33})$. There are 72 rock samples with α_1 real-valued and α_2 complex, 2 rock samples with α_1 and α_2 real-valued. The rock samples collected by Thomsen (1986) and Wang (2002) both demonstrated that it is possible to encounter this type of formation and those pseudo modes should be avoided when performing dispersion extraction.

In geophysical exploration, isotropic formation and VTI formation satisfying the ANNIE approximation (i.e., $c_{13} = c_{33} - 2c_{44}$, $c_{11} = c_{33} + 2(c_{66} - c_{44})$) (Schoenberg et al., 1996) and Thomsen anisotropy parameter $\gamma = \frac{c_{66} - c_{44}}{2c_{44}} > 0$ are commonly encountered. For isotropic formations, α_1 and α_2 are zeros. For VTI formations satisfying the ANNIE approximation and Thomsen anisotropy parameter $\gamma > 0$ (e.g., Tang and Cheng, 2004; Xu et al., 2017, 2018), α_1 and α_2 are complex due to $b^2 - 4ac = 32c_{44}(c_{44} - c_{66})(c_{33} + 2(c_{66} - c_{44}))(c_{33} - c_{44})^3 < 0$. The dispersion curve of real-valued wave modes can be obtained by traditional methods without the influence of pseudo modes.

From the boundary conditions at the fluid–solid interface, the related elements of the dispersion matrix in the wireline tool case (Tang and Cheng, 2004) and the LWD tool case (e.g., Briggs, 2006;

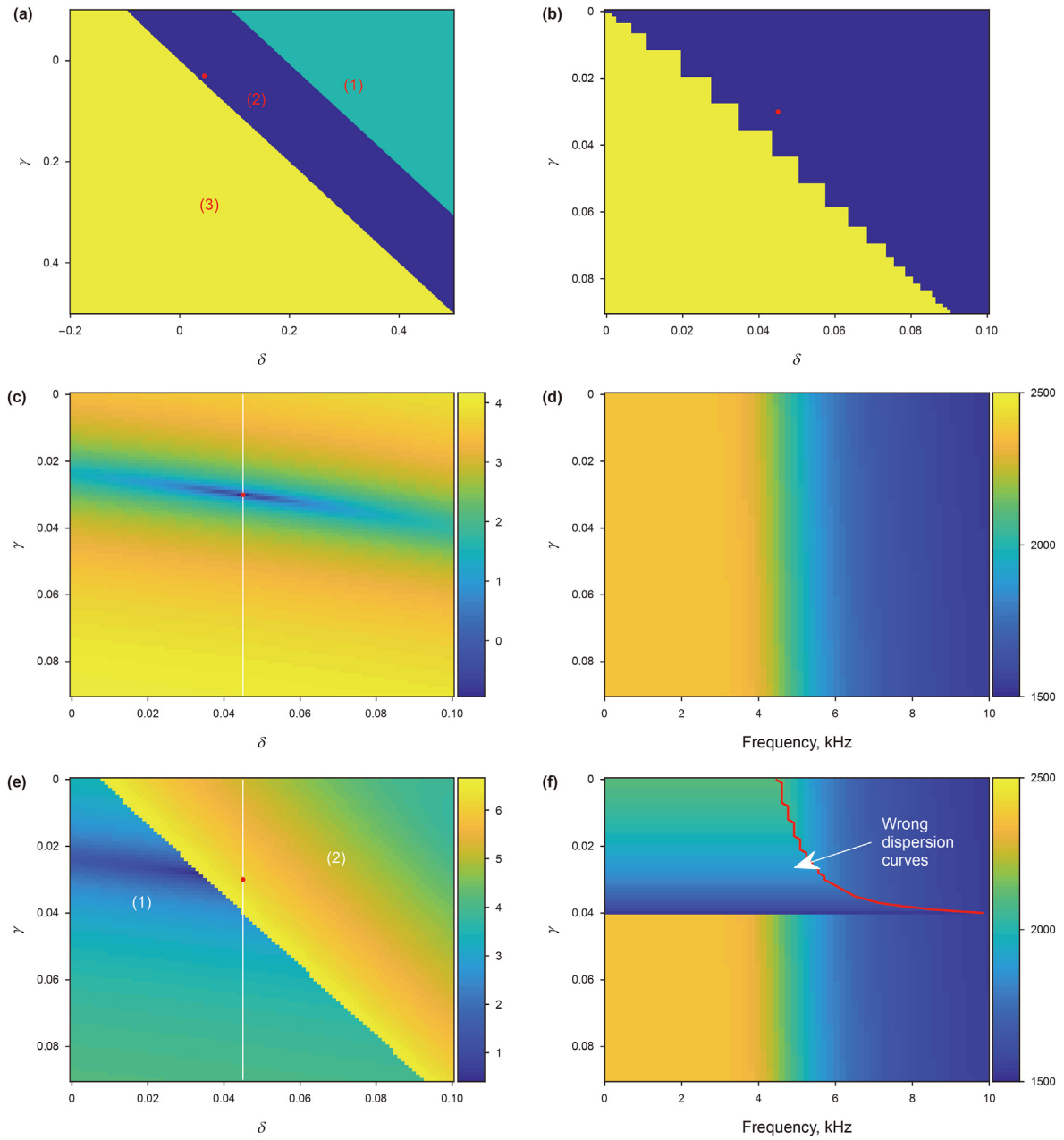

Fig. 7. Bandera sandstone. Distribution of pseudo modes when (a) δ and γ are set as [-0.2, 0.5], [-0.1, 0.5], respectively; (b) δ and γ are set as [0, 0.1], [0, 0.09], respectively; (c) error surfaces of $Obj(\delta,\ \gamma)$ with dispersion curves determined by Eq. (13); (d) dispersion curves determined by Eq. (13) with γ changed from 0 to 0.09 and other Thomsen parameters held; (e) error surfaces of $Obj(\delta,\ \gamma)$ with dispersion curves determined by Eq. (4) with γ changed from 0 to 0.09 and other Thomsen parameters held; (f) dispersion curves determined by Eq. (4).

Zheng, 2012; Li et al., 2013; Wang and Qiao, 2015) are equal to the elements in the conventional dispersion matrix (Tang and Cheng, 2004). Therefore, the method of removing real-valued α_1 and α_2 is also suitable for the dispersion equations in the above two cases. For the LWD tool case, the influence of borehole fluid velocity can also be removed by the same method used in Eq. (13). And the shear velocity of drill collar can also be removed by the similar method considering the asymptotic expansion for the modified Bessel functions of the first kind $I_n(z)$ with small z. Because they are derived from the elements in the same column of dispersion matrix.

5. Conclusion

We have proposed a modified dispersion equation in which the influence of pseudo modes and borehole fluid velocity can be removed successfully. For VTI formations with $\delta \le \varepsilon + c_{44}/(2c_{33})$, pseudo modes α_1 or α_2 derived from $q_P = q_{SV}$ might interfere with dispersion extraction and Thomsen anisotropic parameters inversion. Therefore, these real-valued α_1 and α_2 in some VTI formations with $\delta \le \varepsilon + c_{44}/(2c_{33})$ must be removed when performing dispersion extraction. The influence of α_1 for VTI formation with $\delta > \varepsilon + c_{44}/(2c_{33})$ can also be avoided. The dispersion curves for all VTI formation can be obtained accurately by solving the modified dispersion equation when starting from high frequency with the

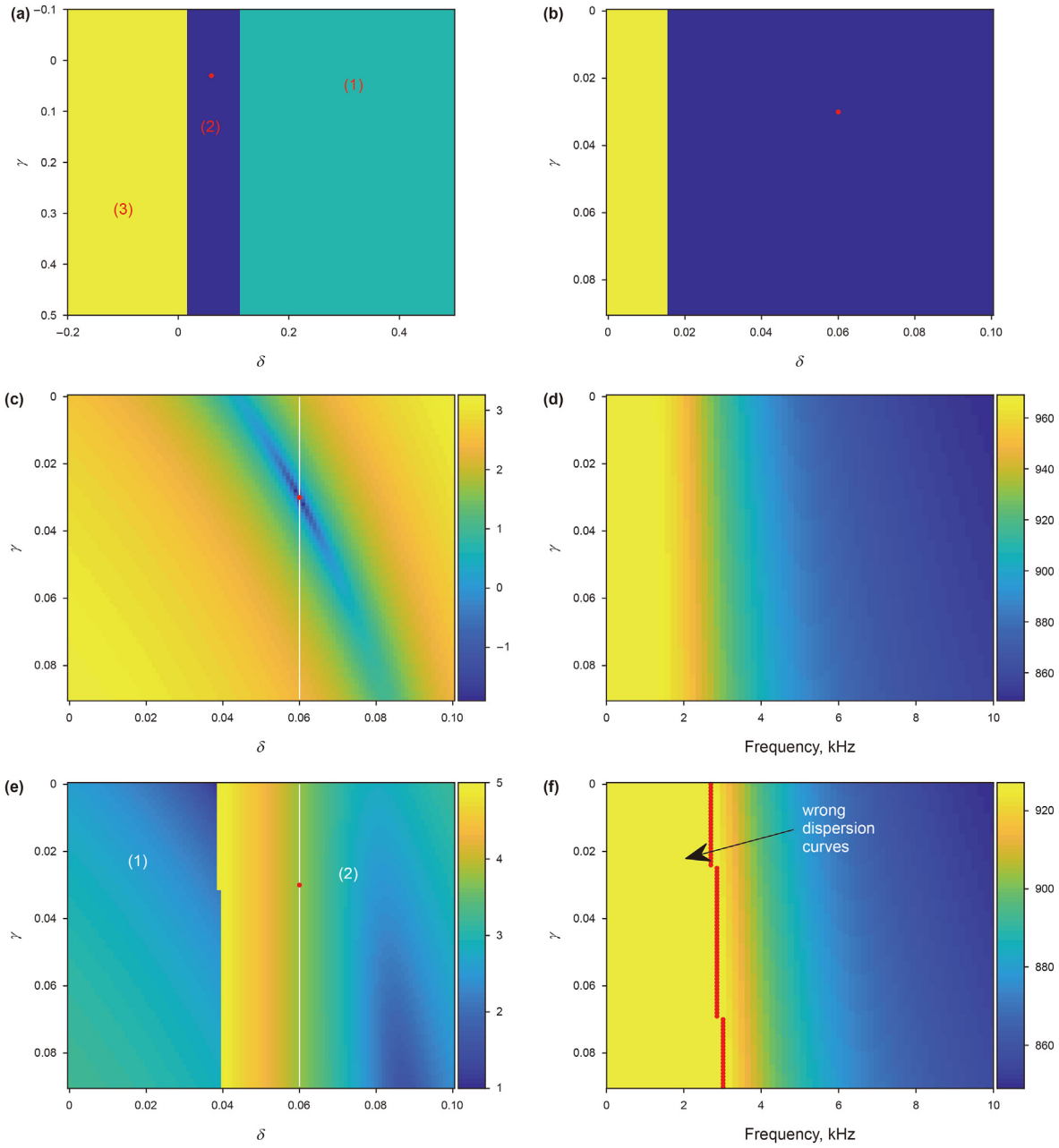

Fig. 8. Pierre shale 950. Distribution of pseudo modes when (a) δ and γ are set as [-0.2, 0.5], [-0.1, 0.5], respectively; (b) δ and γ are set as [0, 0.1], [0, 0.09], respectively; (c) error surfaces of $Obj(\delta,\ \gamma)$ with dispersion curves determined by Eq. (13); (d) dispersion curves determined by Eq. (13) with γ changed from 0 to 0.09 and other Thomsen parameters held; (e) error surfaces of $Obj(\delta,\ \gamma)$ with dispersion curves determined by Eq. (4) with γ changed from 0 to 0.09 and other Thomsen parameters held; (f) dispersion curves determined by Eq. (4).

Scholte wave velocity of VTI formations as an initial guess. In addition, the Scholte wave velocity is dependent on c_{11}, c_{13}, c_{33}, c_{44}, ρ, ρ_f and α_f, but not dependent on c_{66}. Both theoretical analysis and anisotropic parameters inversion in a VTI formation could benefit from more reliable dispersion curves than conventional dispersion equation.

Acknowledgements

We thank the financial support provided by the National Natural Science Foundation of China (Grant No. 42104127 and 42004117) and the Fundamental Research Funds for the Central Universities, China University of Geosciences (Wuhan) (Grant No. 162301192696). We also gratefully acknowledge the helpful comments from the editors and anonymous reviewers, which greatly improved this manuscript.

Appendix A. Elements in A_f

The determinants N and D in reflection coefficient A_f in Eq. (1) are expressed as

$$N=\begin{pmatrix} b_1 & M_{12} & M_{13} & M_{14} \\ b_2 & M_{22} & M_{23} & M_{24} \\ 0 & M_{32} & M_{33} & M_{34} \\ 0 & M_{42} & M_{43} & M_{44} \end{pmatrix} \text{ and } D = \begin{pmatrix} M_{11} & M_{12} & M_{13} & M_{14} \\ M_{21} & M_{22} & M_{23} & M_{24} \\ 0 & M_{32} & M_{33} & M_{34} \\ 0 & M_{42} & M_{43} & M_{44} \end{pmatrix}$$

where,

$$b_1=\varepsilon_n\left[\frac{n}{R}K_n(fR)-fK_{n+1}(fR)\right]$$

$$b_2=-\varepsilon_n\rho_f\omega^2K_n(fR)$$

$$M_{11}=-\frac{n}{R}I_n(fR)-fI_{n+1}(fR)$$

$$M_{12}=-(c_{13}+c_{44})\left[-\frac{n}{R}K_n(q_PR)+q_PK_{n+1}(q_PR)\right]$$

$$M_{13}=\frac{n}{R}K_n(q_{SH}R)$$

$$M_{14}=-ik(c_{13}+c_{44})\left[-\frac{n}{R}K_n(q_{SV}R)+q_{SV}K_{n+1}(q_{SV}R)\right]$$

$$M_{21}=\rho_f\omega^2I_n(fR)$$

$$M_{22}=\left[c_{11}c_{44}q_P^2+c_{13}\left(c_{44}k^2-\rho\omega^2\right)\right]K_n(q_PR)+\frac{2c_{66}(c_{13}+c_{44})}{R}\left[\frac{n(n-1)}{R}K_n(q_PR)+q_PK_{n+1}(q_PR)\right]$$

$$M_{23}=\frac{2nc_{66}}{R}\left[\frac{n(n-1)}{R}K_n(q_{SH}R)-q_{SH}K_{n+1}(q_{SH}R)\right]$$

$$M_{24}=ik\left\{\left[c_{11}c_{44}q_{SV}^2+c_{13}\left(c_{44}k^2-\rho\omega^2\right)\right]K_n(q_{SV}R)+\frac{2c_{66}(c_{13}+c_{44})}{R}\left[\frac{n(n-1)}{R}K_n(q_{SV}R)+q_{SV}K_{n+1}(q_{SV}R)\right]\right\}$$

$$M_{31}=0$$

$$M_{32}=\frac{2nc_{66}}{R}(c_{13}+c_{44})\left[\frac{1-n}{R}K_n(q_PR)+q_PK_{n+1}(q_PR)\right]$$

$$M_{33}=-c_{66}\left\{\left[\frac{2n(n-1)}{R^2}+q_{SH}^2\right]K_n(q_{SH}R)+\frac{2q_{SH}}{R}K_{n+1}(q_{SH}R)\right\}$$

$$M_{34}=\frac{2nc_{66}}{R}ik(c_{13}+c_{44})\left[\frac{1-n}{R}K_n(q_{SV}R)+q_{SV}K_{n+1}(q_{SV}R)\right]$$

$$M_{41}=0$$

$$M_{42}=\frac{c_{44}}{ik}\left(c_{13}k^2+c_{11}q_P^2+\rho\omega^2\right)\left[-\frac{n}{R}K_n(q_PR)+q_PK_{n+1}(q_PR)\right]$$

$$M_{43}=\frac{iknc_{44}}{R}K_n(q_{SH}R)$$

$$M_{44}=c_{44}\left(c_{13}k^2+c_{11}q_{SV}^2+\rho\omega^2\right)\left[-\frac{n}{R}K_n(q_{SV}R)+q_{SV}K_{n+1}(q_{SV}R)\right]$$

ε_n is the Neumann coefficient, I_n and K_n is the modified Bessel function of the first and second kind, respectively. The radial wavenumbers for the borehole fluid and the formation quasi-P, quasi-S and horizontally polarized shear (SH) waves are given by $f=\sqrt{k^2-(\omega/\alpha_f)^2}$, $q_P=\omega\sqrt{(-V+\sqrt{V^2-4UW})/(2U)}$, $q_{SV}=\omega\sqrt{(-V-\sqrt{V^2-4UW})/(2U)}$ and $q_{SH}=\sqrt{(c_{44}k^2-\rho\omega^2)/c_{66}}$, where the symbols U, V and W are given by

$$U=c_{11}c_{44},$$

$$V=\rho(c_{11}+c_{44})+\left(c_{13}^2+2c_{13}c_{44}-c_{11}c_{33}\right)\left(k^2\,/\,\omega^2\right),$$

$$W=\left(\rho-c_{44}k^2\,/\,\omega^2\right)\left(\rho-c_{33}k^2\,/\,\omega^2\right).$$

Appendix B. Elements M_{ij}^0

Considering the asymptotic expansion for the modified Bessel functions of the first and second kind (Zhang and Jin, 2011), when $\omega\to0$, M_{ij} after removing common factors can be simplified as M_{ij}^0. For $n=0$, M_{ij}^0 is expressed as

$$M_{11}^0=-f^2,$$

$$M_{12}^0=-ik(c_{13}+c_{44}),$$

$$M_{14}^0=-ik(c_{13}+c_{44}),$$

$$M_{21}^0=2\rho_f\omega^2,$$

$$M_{22}^0=ik\left\{2c_{66}(c_{13}+c_{44})-R^2\left[c_{11}c_{44}q_P^2-c_{13}\left(\rho\omega^2-c_{44}k^2\right)\times\right]\ln(q_PR)\right\},$$

$$M_{24}^0=ik\left\{2c_{66}(c_{13}+c_{44})-R^2\left[c_{11}c_{44}q_{SV}^2-c_{13}\left(\rho\omega^2-c_{44}k^2\right)\times\right]\ln(q_{SV}R)\right\},$$

$$M_{33}^0=c_{66}\left[R^2q_{SH}^2\ln(q_{SH}R)-2\right],$$

$$M_{42}^0=c_{13}k^2+c_{11}q_P^2+\rho\omega^2,$$

$$M_{44}^0=c_{13}k^2+c_{11}q_{SV}^2+\rho\omega^2,$$

$$M_{13}^0=M_{23}^0=M_{31}^0=M_{32}^0=M_{34}^0=M_{41}^0=M_{43}^0=0.$$

For $n>0$, M_{ij}^0 is expressed as

$$M_{11}^0 = -\left[\frac{2n}{\Gamma(n+1)} + \frac{(fR)^2}{\Gamma(n+2)}\right],$$

$$M_{12}^0 = ik(c_{13}+c_{44})[n\Gamma(n) - 2\Gamma(n+1)],$$

$$M_{13}^0 = n\Gamma(n),$$

$$M_{14}^0 = ik(c_{13}+c_{44})[n\Gamma(n) - 2\Gamma(n+1)],$$

$$M_{21}^0 = \frac{\rho_f\omega^2}{\Gamma(n+1)},$$

$$M_{22}^0 = ik\left\{\left[c_{11}c_{44}q_P^2 - c_{13}\left(\rho\omega^2 - c_{44}k^2\right)\right] \times \right]\frac{\Gamma(n)}{2} + \frac{c_{66}}{R^2}(c_{13}+c_{44})[2\Gamma(n+1) + n(n-1)\Gamma(n)]\right\},$$

$$M_{23}^0 = \frac{nc_{66}}{R^2}[(n-1)\Gamma(n) - 2\Gamma(n+1)],$$

$$M_{24}^0 = ik\left\{\left[c_{11}c_{44}q_{SV}^2 - c_{13}\left(p\omega^2 - c_{44}k^2\right)\right]\frac{\Gamma(n)}{2} + \frac{c_{66}}{R^2}(c_{13}+c_{44})[2\Gamma(n+1) + n(n-1)\Gamma(n)]\right\},$$

$$M_{31}^0 = 0,$$

$$M_{32}^0 = ink(c_{13}+c_{44})[2\Gamma(n+1) - (n-1)\Gamma(n)],$$

$$M_{33}^0 = \left[2n(1-n) - q_{SH}^2R^2\right]\Gamma(n) - 2\Gamma(n+1),$$

$$M_{34}^0 = ink(c_{13}+c_{44})[2\Gamma(n+1) - (n-1)\Gamma(n)],$$

$$M_{41}^0 = 0,$$

$$M_{42}^0 = \left(c_{13}k^2 + c_{11}q_P^2 + \rho\omega^2\right)[2\Gamma(n+1) - n\Gamma(n)],$$

$$M_{43}^0 = ink\Gamma(n),$$

$$M_{44}^0 = \left(c_{13}k^2 + c_{11}q_{SV}^2 + \rho\omega^2\right)[2\Gamma(n+1) - n\Gamma(n)],$$

where $\Gamma(n)$ is the gamma function (Zhang and Jin, 2011).

References

Braunisch, H., Habashy, T.M., Sinha, B.K., et al., 2004. Inversion of guided wave dispersion data with application to borehole acoustics. J. Acoust. Soc. Am. 115 (1), 269–279. https://doi.org/10.1121/1.1625683.

Briggs, V.A., 2006. A Comparison of Logging while Drilling (LWD) and Wireline Acoustic Measurements. Ph. D. dissertation. Massachusetts Institute of Technology, Cambridge.

Fang, X.D., Cheng, A., 2018. Detection of formation S-wave in a slow formation using a monopole acoustic logging-while-drilling tool. Geophys. Nor. 83 (1), D9–D16. https://doi.org/10.1190/geo2017-0300.1.

He, X., Hu, H.S., 2009. Borehole flexural modes in transversely isotropic formations: low-frequency asymptotic velocity. Geophys. Nor. 74 (4), E149–E158. https://doi.org/10.1190/1.3141442.

He, X., Hu, H.S., 2010. Single-valued definition of the multivalued function for borehole acoustic waves in transversely isotropic formations. Sci. China Phys. Mech. Astron. 53, 1419–1426. https://doi.org/10.1007/s11433-010-4037-7.

Ingber, L., 1989. Very fast simulated re-annealing. Math. Comput. Model. 12, 967–973. https://doi.org/10.1016/0895-7177(89)90202-1.

Jiang, C., Zhuang, C.X., Li, S.Q., et al., 2019. Joint inversion for compressional and shear wave slowness using multipole acoustic array logging data. Chin. J. Geophys. 62 (6), 2294–2302. https://doi.org/10.6038/cjg2019L0714 (in Chinese).

Kimball, C.V., Marzetta, T.L., 1986. Semblance processing of borehole acoustic array data. Geophys. Nor. 49 (3), 274–281. https://doi.org/10.1190/1.1441659.

Li, W., Tao, G., Matuszyk, P.J., et al., 2015. Forward and backward amplitude and phase estimation method for dispersion analysis of borehole sonic measurements. Geophys. Nor. 80 (3), D295–D308. https://doi.org/10.1190/geo2014-0298.1.

Li, X.Q., Chen, H., He, X., et al., 2013. Analyses on mode waves of acoustic logging while drilling in transversely isotropic formations. Chin. J. Geophys. 56 (9), 3212–3222. https://doi.org/10.6038/cjg20130933 (in Chinese).

Ma, M.M., Chen, H., He, X., et al., 2013. The inversion of shear wave slowness's radial variations based on dipole flexural mode. Chin. J. Geophys. 56 (6), 2077–2087. https://doi.org/10.6038/cjg20130628 (in Chinese).

Moré, J.J., 1978. The Levenberg-Marquardt algorithm: implementation and theory. Numerical analysis 105–116.

Müller, T.M., Gurevich, B., Lebedev, M., 2010. Seismic wave attenuation and dispersion resulting from wave-induced flow in porous rocks—a review. Geophys. Nor. 75 (5), A147–A164. https://doi.org/10.1190/1.3463417.

Press, W.H., Teukolsky, S.A., Vetterling, W.T., et al., 2007. Numerical Recipes. Cambridge University Press, UK.

Schmitt, D.P., 1988. Shear wave logging in elastic formation. J. Acoust. Soc. Am. 84 (6), 2215–2229. https://doi.org/10.1121/1.397015.

Shmakov, S.L., 2011. A universal method of solving quartic equations. Int. J. Pure Appl. Math. 71 (2), 251–259.

Schoenberg, M., Muir, F., Sayers, C.M., 1996. Introducing ANNIE: a simple three-parameter anisotropic velocity model for shales. J. Seismic Explor. 5, 35–49.

Sinha, B.K., Asvadurov, S., 2004. Dispersion and radial depth of investigation of borehole modes. Geophys. Prospect. 52 (4), 271–286. https://doi.org/10.1111/j.1365-2478.2004.00415.x.

Sunaga, S., Sinha, B.K., Endo, T., et al., 2009. Radial Profiling of Shear Slownesses in TIV Formations. SEG Technical Program Expanded Abstracts, pp. 3481–3484. https://doi.org/10.1190/1.3255586.

Tang, X.M., Cheng, C.H., 2004. Quantitative Borehole Acoustic Methods. Elsevier Science Publishing, Amsterdam.

Thomsen, L., 1986. Weak elastic anisotropy. Geophys. Nor. 51 (10), 1954–1966. https://doi.org/10.1190/1.1442051.

Tsang, L., Radar, D., 1979. Numerical evaluation of the transient acoustic waveform due to a point source in a fluid-filled borehole. Geophys. Nor. 44 (10), 1706–1720. https://doi.org/10.1190/1.1440932.

Valero, H.P., Djikpesse, H.A., Sinha, B.K., 2009. Estimation of Borehole Fluid Slowness Using Sonic Array Waveforms. SEG Technical Program Expanded Abstracts, pp. 361–364. https://doi.org/10.1190/1.3255617.

Vinh, P.C., 2013. Scholte-wave velocity formulae. Wave Motion 50 (2), 180–190. https://doi.org/10.1016/j.wavemoti.2012.08.006.

Wang, R.J., Qiao, W.X., 2015. Numerical study on quadrupole acoustic LWD in VTI formations. Chin. J. Geophys. 58 (8), 2862–2872. https://doi.org/10.6038/cjg20150820 (in Chinese).

Wang, Z., 2002. Seismic anisotropy in sedimentary rocks, part 2: laboratory data. Geophys. Nor. 67 (5), 1423–1440. https://doi.org/10.1190/1.1512743.

White, J.E., Sengbush, R.L., 1953. Velocity measurements in near-surface formations. Geophys. Nor. 18 (1), 54–69. https://doi.org/10.1190/1.1437863.

Xu, S., Tang, X.M., Su, Y.D., et al., 2017. Determining formation S-wave transverse isotropy from borehole flexural-wave dispersion data. Geophys. Nor. 82 (2), D47–D55. https://doi.org/10.1190/geo2016-0223.1.

Xu, S., Tang, X.M., Su, Y.D., et al., 2018. Determining formation shear wave transverse isotropy jointly from borehole Stoneley-and flexural-wave data. Chin. J. Geophys. 61 (12), 5105–5114. https://doi.org/10.6038/cjg2018L0521 (in Chinese).

Zeng, F., 2019. Identification and Estimation of Abnormal Principal Horizontal Stresses in Isotropic Formation Using Borehole Sonic Data. Ph. D. thesis. China University of Petroleum-Beijing, Beijing. https://doi.org/10.27643/d.cnki.gsybu.2019.000134 (in Chinese).

Zhang, B., Dong, H., Wang, K., 1994. Multipole sources in a fluid-filled borehole surrounded by a transversely isotropic elastic solid. J. Acoust. Soc. Am. 96 (4), 2546–2555. https://doi.org/10.1121/1.411383.

Zhang, C., Hu, H., Zheng, X., 2019. Inversion of shear wave velocity in slow formation by dipole Scholte wave during acoustic logging while drilling. Chin. J. Geophys. 62 (6), 2286–2293. https://doi.org/10.6038/cjg2019M0288 (in Chinese).

Zhang, S.J., Jin, J.M., 2011. Computation of Special Functions. Nanjing University

Press, Nanjing (in Chinese).
Zhang, X.M., Zhang, H.L., Wang, X.M., 2009. Acoustic mode waves and individual arrivals excited by a dipole source in fluid-filled boreholes. Sci. China Ser. G-Phys Mech. Astron. 52 (6), 822–831. https://doi.org/10.1007/s11433-009-0090-5.
Zhao, L., Cao, C., Yao, Q., et al., 2020. Gassmann consistency for different inclusion-based effective medium theories: implications for elastic interactions and poroelasticity. J. Geophys. Res. Solid Earth 125 (3), e2019JB018328. https://doi.org/10.1029/2019JB018328.
Zhao, L., Han, D., Yao, Q., et al., 2015. Seismic reflection dispersion due to wave-induced fluid flow in heterogeneous reservoir rocks. Geophys. Nor. 80 (3), D221–D235. https://doi.org/10.1190/geo2014-0307.1.
Zhao, L., Wang, Y., Yao, Q., et al., 2021. Extended gassmann equation with dynamic volumetric strain: modeling wave dispersion and attenuation of heterogenous porous rocks. Geophys. Nor. 86 (3), MR149–MR164. https://doi.org/10.1190/geo2020-0395.1.
Zheng, X., 2012. The Full-Waveform Simulation of Acoustic Logging while Drilling. Master Dissertation. Harbin Institute of Technology, Harbin (in Chinese). https://kns.cnki.net/KCMS/detail/detail.aspx?dbname=CMFD201401&filename=1013037285.nh.